The International Journal of Advanced Manufacturing Technology (2020) 110:1153–1161
https://doi.org/10.1007/s00170-020-05867-w

ORIGINAL ARTICLE

# NC machining verification algorithm based on the STL model

Ying Miao[1,2] · Xiaowen Song[3] · Jun Wang[1,2] · Zhonghua Lu[1,2]

Received: 29 April 2020 / Accepted: 31 July 2020 / Published online: 20 August 2020

## Abstract

An algorithm to assess the deviation of a machined workpiece model for a nominal part of the stereolithography (STL) model-based numerically controlled (NC) machining verification is presented, which is inspired by several algorithms used for evaluating the difference between two triangular meshes of similar shape, and some improvements are made. First, each triangle of the machined workpiece model is sampled under a user-defined sampling step $\delta$. Then, the signed distance between each sample and the nominal part is computed to obtain the maximal error, minimal error, and mean error between the two STL models. Finally, a background grid is constructed to quickly search for the triangle closest to the sampling point. The experimental results demonstrate that the accuracy can be improved by sampling all the triangles, including those too small to be sampled under the current sampling step $\delta$. The efficiency can be increased by applying a background grid, and the undercut and overcut areas can be easily detected by coloring the machined workpiece model according to the signed distance associated with each sample.

**Keywords** NC machining verification · STL model · Sampling step · Signed distance · Background grid

## 1 Introduction

NC machining simulation, which simulates and evaluates the actual NC machining process via computer graphics, has become an important step in modern manufacturing. By simulating the machining process prior to the actual cutting operation, inefficiency and errors in the tool path can be reduced and corrected at the programming stage. NC machining simulation technology contains two aspects: material removal process simulation and NC machining verification. The material removal process simulation realized via consecutive Boolean subtractions between the updated workpiece and the cutter swept volume is used to detect collisions and predict the final workpiece shape. NC machining verification algorithms are used to compare the geometrical differences between the simulated workpiece and the nominal part and to estimate whether the difference is within the allowable tolerance zone. NC machining simulation methods can be categorized into four major approaches according to the workpiece representation model, including the solid-based approach, object space-based approach, image space-based approach, and hybrid approach.

In the solid-based approach, the workpiece is represented by a constructive solid geometry (CSG) [1] or boundary representation (B-rep) model [2]. The material removal process is simulated by an explicit Boolean subtraction operation between the workpiece model and cutter swept volume [3], and verification is achieved by calculating the Boolean differences between the workpiece model and the nominal part. The solid-based approach can provide a precise and detailed geometric representation but requires heavy computational efforts[4], as the computation cost is reported to be O($n^4$) in the worst case using CSG and estimated to be O($n^{1.5}$) using the B-rep, where $n$ is the number of cutter movements [2].

In the object space-based approach, the workpiece is approximately represented by a collection of basic geometric elements within the given accuracy. The object space-based approach can be further classified into the Z-map-based [5], vector-based [6], and voxel-based [7] approaches, where the workpiece is represented by three-dimensional (3D)

✉ Xiaowen Song
songxw@zju.edu.cn

[1] Mechanical Institute of Technology, Wuxi Institute of Technology, Wuxi 214121, China

[2] Jiangsu Intelligent Production Line Technology and Equipment Engineering Research Center, Wuxi Institute of Technology, Wuxi 214121, China

[3] State Key Laboratory of Fluid Power and Mechatronic System, College of Mechanical Engineering, Zhejiang University, Hangzhou 310027, China

histograms, surface points with vectors, and cubic cells, respectively. The object space-based approach suffers from the conflict between simulation accuracy and efficiency because the accuracy enhancement is inevitably accompanied by drastically increased computation time and memory consumption [8].

In the image space-based approach, the workpiece and cutter swept volume are represented by the depth pixel (called dexel) model. The material removal process simulation is performed in one-dimensional (1D) space by comparing the depth value of the pixels. Wang and Wang [9] were the first to apply the dexel model to real-time NC machining simulation. More recently, Sun et al. [10] applied the triple-dexel model, which contains the dexel information in the *X*, *Y*, and *Z* directions, to verify the effectiveness of the tool path in a 5-axis hybrid additive-subtractive manufacturing simulation. Since Boolean operations are performed in 1D space by comparing the depth value of the pixels, the image space-based approach is the fastest among all the simulation approaches. However, a true solid model of the updated workpiece is not directly available.

To take advantage of different workpiece representations, some studies adopted hybrid representations. Karunakaran and Shringi implemented an algorithm for converting the octree into B-rep [11] and applied the algorithm in their NC simulation system [12], where the workpiece is always stored as an octree model and the user can convert it into a B-rep for visual and dimensional verification. Yau and Tsou [13] used an octree-based voxel representation to save a significant amount of memory and constructed a triangular mesh from the voxel data to provide high-resolution and smooth displays. Lee and Nestler [14] adopted the triple-dexel model to represent the workpiece and then reconstructed a triangular mesh from the sampled data by recognizing the feature-sensitive geometries. In any case, those systems only provide approximate results for performance optimization.

The authors of this paper proposed an efficient STL model-based NC machining simulation approach [15], where both the workpiece and cutter swept volume are represented by STL models and the cutting process is simulated by performing consecutive Boolean subtractions between the two STL models. The STL model-based approach can generate an exact workpiece model, and the efficiency was improved by applying two spatial decomposition methods: workpiece division and background grid. In this work, the authors extended their previous work to investigate the NC machining verification approach by comparing the STL models of the machined workpiece and the nominal part, both of which are represented by a triangular mesh.

The rest of the paper is organized as follows. Some related work is briefly reviewed in Section 2. The details of the proposed algorithm for NC machining verification are described in Section 3. The experimental results of the algorithm accuracy and efficiency are discussed in Section 4. Finally, the conclusion is given in Section 5.

## 2 Related work

The core of NC machining verification is computing a distance measure between two geometric models, which is an important problem in diverse fields, including computer graphics, virtual environment, and geometric modeling. Various types of distance measures have been extensively investigated, and efficient algorithms have been proposed over the past two decades [16].

Metro [17] and MESH [18] are the earliest methods applied to evaluate the distance between two triangular meshes of similar shape by sampling each triangle of one mesh and computing the distance between each sample and the other mesh. However, no sampling analysis is provided, and triangles that have an area smaller than the sampling step are not sampled; thus, relevant details in the models' shape are missed.

Tang et al. [16] presented a fast and simple algorithm to compute the Hausdorff distance between complicated polygonal models at interactive rates, and the computed distance is an approximation within a user-specified error bound. The algorithm was implemented by calculating tight upper and lower bounds for the exact Hausdorff distance value and then refining these bounds through polygon subdivision until the error bound was obtained. The algorithm is sensitive to the relative configuration of the objects, and its space complexity tends to infinity as the Hausdorff distance decreases.

Bartoň et al. [19] presented an exact algorithm for computing the precise Hausdorff distance between triangular meshes. The bisectors of the pairs of primitives (i.e., vertex, edge, or face) are analytically constructed and intersected with the other mesh, yielding a set of conic segments. For each conic segment, the distance functions to all of the primitives are constructed, and the maximum value of their low envelope function may correspond to a candidate point for the Hausdorff distance. Due to the high complexity, the worst-case time complexity was O ($n^4$ log $n$) with a complete implementation.

Kang et al. presented an algorithm that computes the one-sided Hausdorff distance from a triangle mesh to a quad mesh using what is called "matching" and "upper bounding" of the candidate pieces [20]. Then, they completed the algorithm by computing the one-sided Hausdorff distance in the opposite direction: from the quad mesh to the triangle mesh [21]. Combining the two one-sided computational algorithms, the two-sided Hausdorff distance between the two meshes can be computed and used to evaluate a quad mesh approximation for a triangle mesh.

To realize the verification algorithm in the STL model-based NC machining, where both the machined workpiece and the nominal part are represented by a triangular mesh, we adopt some ideas used in Metro [17] and MESH [18] and make some improvements. First, the definition of the signed distance introduced in Metro [17] is adopted in this work because it can be used to evaluate whether the workpiece is undercut or overcut. Second, the sampling lattice used in MESH [18] is also adopted since it leads to significantly simpler computations of integrals over a surface. In addition, to avoid the loss of detail features, the three vertices of a triangle whose area is very small are treated as the sample points, so that each triangle in the STL model will be sampled and the computed distance will be more accurate.

## 3 The algorithm

The overall algorithm for NC machining verification, as shown in Fig. 1, consists of three steps as follows:

Step 1 : Each triangle of the machined workpiece model is sampled under a user-defined sampling step.

Step 2 : The signed distance between each sample and the nominal part is computed, and thus, the maximal error, minimal error, and mean error between the two STL models are evaluated.

Step 3 : A 3D background grid is constructed to quickly search for the triangle closest to the sampling point, and therefore, the algorithm efficiency is improved.

### 3.1 Surface sampling

The first step of the algorithm is to sample each triangle of the machined workpiece model, which is achieved in the following way: two sides of the triangle are considered as the directions for the sampling lattice, as shown in Fig. 2. According to a given sampling step $\delta$, each side is sampled with $n$ points, and the number of samples in each triangle is $n(n+1)/2$. The smaller the sampling step, the greater the number of sampling points there are in each triangle, so the algorithm results will be more accurate, but the algorithm efficiency will be lower.

Here, the sampling step $\delta$ is an important parameter that will affect the efficiency and accuracy of the algorithm. The relationships between efficiency and accuracy will be discussed in Section 4. Given the sampling step $\delta$, $n'$ is defined as:

$$n' = \sqrt{\frac{1}{4} + \frac{2|T_1|}{\delta^2}} - \frac{1}{2} \qquad (1)$$

where $|T_1|$ is the area of the triangle. In general, $n'$ is not an integer. The number $n$ of samples on each triangle side is obtained by rounding $n'$ to an integer. If $\delta$ is relatively large and $|T_1|$ is relatively small, the computed $n$ will be 0 or 1, which means that the triangle will not be sampled. For models with a large number of triangles, the proportion of these unsampled triangles is non-negligible, and thus, the accuracy of the algorithm results will be affected. Especially in the machined workpiece model, tiny triangles accumulate at the cusps between the tool paths, as shown in Fig. 3. If these tiny triangles are not sampled, the results of the NC machining verification algorithm are not accurate. To obtain accurate results, $n$ will be set to 2 if the computed $n$ is less than 2, which means that the three vertices of the triangle are taken as the samples when the triangle is too small to be sampled under the current sampling step $\delta$.

The coordinates of the samples on each triangle are defined as:

$$P(i,j) = P_A + i\,\vec{e_1} + j\,\vec{e_2} \qquad (2)$$

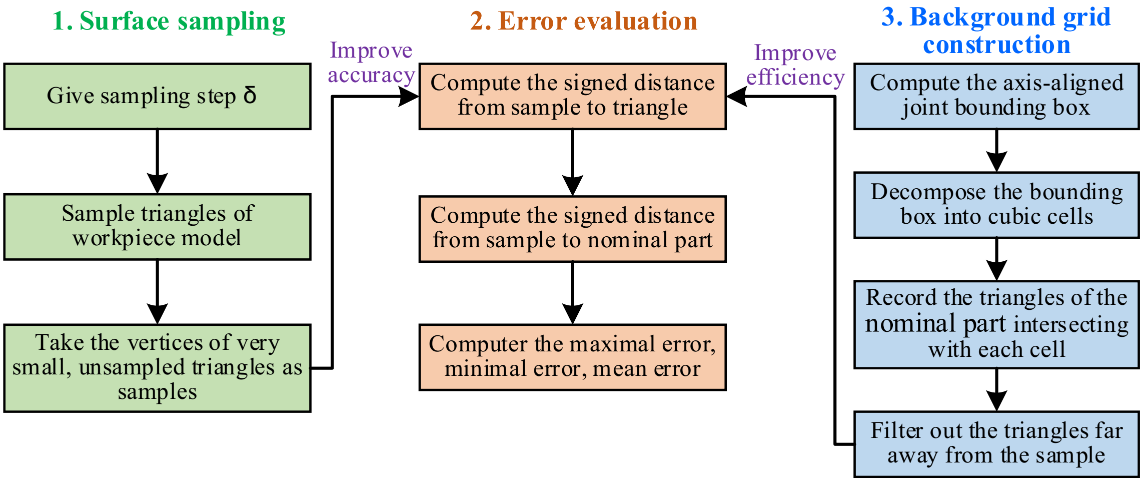
1. Surface sampling
2. Error evaluation
3. Background grid construction
Give sampling step δ
Sample triangles of workpiece model
Take the vertices of very small, unsampled triangles as samples
Improve accuracy
Compute the signed distance from sample to triangle
Compute the signed distance from sample to nominal part
Computer the maximal error, minimal error, mean error
Improve efficiency
Compute the axis-aligned joint bounding box
Decompose the bounding box into cubic cells
Record the triangles of the nominal part intersecting with each cell
Filter out the triangles far away from the sample

**Fig. 1** The overall scheme of the NC machining verification algorithm

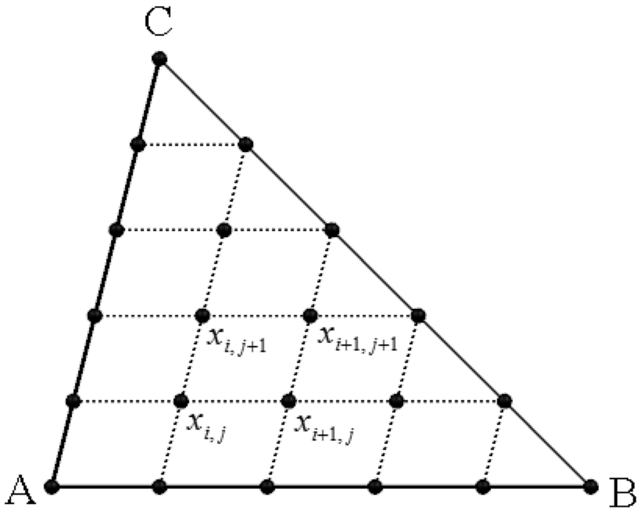

**Fig. 2** Illustration of a sampling performed on triangles for $n = 6$

where $0 \leq i \leq n-1$, $0 \leq j \leq n-1-i$, $\vec{e_1} = (P_B - P_A)\ /(n-1)$, and $\vec{e_2} = (P_C - P_A)\ /(n-1)$.

### 3.2 Error evaluation

After the triangles of the machined workpiece model are sampled, the signed distance between each sample and the nominal part can be defined as follows.

Given sample $p$ of machined workpiece model $S_1$ and triangle $T_2$ of nominal part $S_2$, the signed distance $d(p, T_2)$ between $p$ and $T_2$ is defined as:

$$|d(p, T_2)| = \|p - p_{\min}\|_2 \tag{3}$$

where $p_{\min}$ is the closest point in $T_2$ to $p$ and $\|\|_2$ denotes the usual Euclidean norm. The sign of $d(p, T_2)$ is measured by the sign of $N_p * (p_{min} - p)$. If sample $p$ is outside $S_2$, the sign is positive; otherwise, the sign is negative.

The signed distance $d(p, S_2)$ between $p$ and $S_2$ is defined as:

$$|d(p, S_2)| = \min_{T_2 \in S_2} |d(p, T_2)| \tag{4}$$

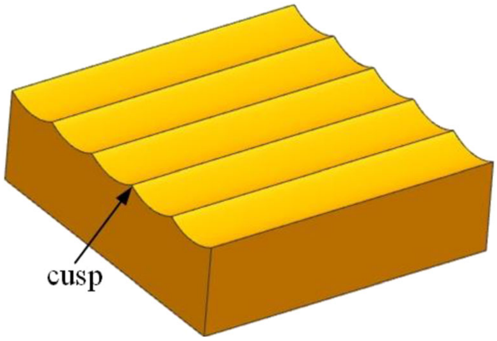

**Fig. 3** An example of the cusp at the machined workpiece model

The sign of $d(p, S_2)$ is defined as mentioned above. $d(p, S_2)$ can be used to represent the error value associated with each sample.

The signed distance defined in (4) can be used to define maximal error $d_{\max}(S_1, S_2)$, minimal error $d_{\min}(S_1, S_2)$, and mean error $d_{\text{mean}}(S_1, S_2)$ as follows.

$$d_{\max}(S_1, S_2) = \max_{p \in S_1} d(p, S_2) \tag{5}$$

$$d_{\min}(S_1, S_2) = \min_{p \in S_1} d(p, S_2) \tag{6}$$

$$d_{\text{mean}}(S_1, S_2) = \frac{1}{|S_1|} \iint_{p \in S_1} d(p, S_2) dS \tag{7}$$

where $|S_1|$ is the total surface area of $S_1$. Here, $d_{\max}(S_1, S_2)$ and $d_{\min}(S_1, S_2)$ can be used to detect the undercut and overcut, respectively, if they fall out of the allowable tolerance zone.

The computation of the integral defined in (7) is not too difficult thanks to the sampling lattice, as shown in Fig. 2. The integral of error defined in (7) is computed approximately by linear interpolation. Three samples of $T_1 \in S_1$, which are denoted as $x_{i,\ j}$, $x_{i+1,\ j}$, and $x_{i,\ j+1}$, constitute a smaller triangle $T_{i,\ j}$. The integral of the error over $T_{i,\ j}$ is denoted as:

$$|T_{i,j}| \times \frac{e_{i,j} + e_{i+1,j} + e_{i,j+1}}{3} \tag{8}$$

where $e_{i,\ j}$, $e_{i+1,\ j}$, and $e_{i,\ j+1}$ are the error values associated with $x_{i,\ j}$, $x_{i+1,\ j}$, and $x_{i,\ j+1}$, respectively. Therefore, the integral of the error defined in (7) can be obtained by the summation of the integrals of the error over all the smaller triangles.

### 3.3 Background grid

The evaluation of the signed distances between each sample and the nominal part is very time-consuming if all the triangles of the nominal part are transversed. The background grid technique [22] can be used to quickly search for the triangle closest to the sampling point.

The construction of the background grid begins with the axis-aligned joint bounding box of $S_1$ and $S_2$, which is then decomposed into cubic cells of uniform size. For each cell, the cell-triangle intersection test can be efficiently computed by using the separating axis theorem [23], and the list of triangles of $S_2$ intersecting with the cell is recorded.

For each sampling point $p$, the cell in which $p$ is located is denoted by $C$. $D_{\text{m}}(C)$ represents the set of cells that are at a distance $m * \Delta d$ from $C$ along with one of the coordinate axes, where $\Delta d$ is the side length of the cubic cells and $m$ is the layer number of cells around $C$, as shown in Fig. 4. First, the distances from $p$ to all the triangles intersecting $C$ are calculated, and the minimum distance $d_{\min}$ is retained. Then, the adjacent cells in $D_{\text{m}}(C)$ are processed by increasing the value of $m$, and $d_{\min}$ is updated accordingly until $d_{\min}$ is smaller than $m * \Delta d$.

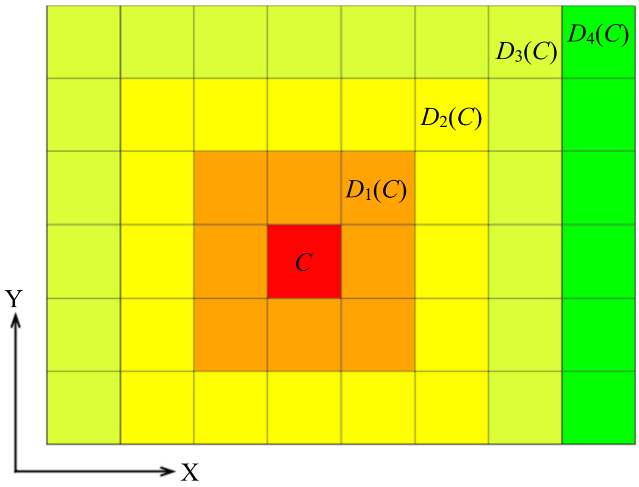

**Fig. 4** An example of a 3D uniform grid represented in two dimensions

As shown in Fig. 5, the sample is located in cell $C$, and the minimum distance from the sample to the triangles intersecting with $C$ is *dis1*, which is assigned to the current $d_{\min}$. Then, the first layer of cells $D_1(C)$ around $C$ is traversed, and the blue cell shown in Fig. 5 is a cell of $D_1(C)$. The minimum distance from the sample to the triangles intersecting with $D_1(C)$ is *dis2*. Since *dis2* is smaller than *dis1*, the current $d_{\min}$ is updated as *dis2*. Furthermore, as the current $d_{\min}$ is smaller than $1 * \Delta d$, the second layer of cells $D_2(C)$ around $C$ does not need to be traversed. Therefore, the minimum distance from the sample to the nominal part is determined and equals *dis2*.

Here, $\Delta d$ is an important parameter for constructing the background grid to improve algorithm efficiency. It should be chosen carefully so that the increase in speed gained by using uniform cells is in equilibrium with the overhead of handling them. Empirically, the side length of an average triangle, which is an equilateral triangle that has an area equal to the average triangle area of $S_2$, is a reasonable value in most cases.

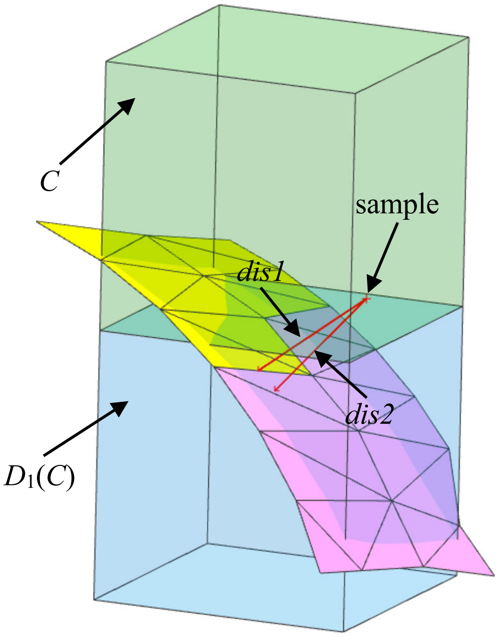

**Fig. 5** An example of the minimum distance update

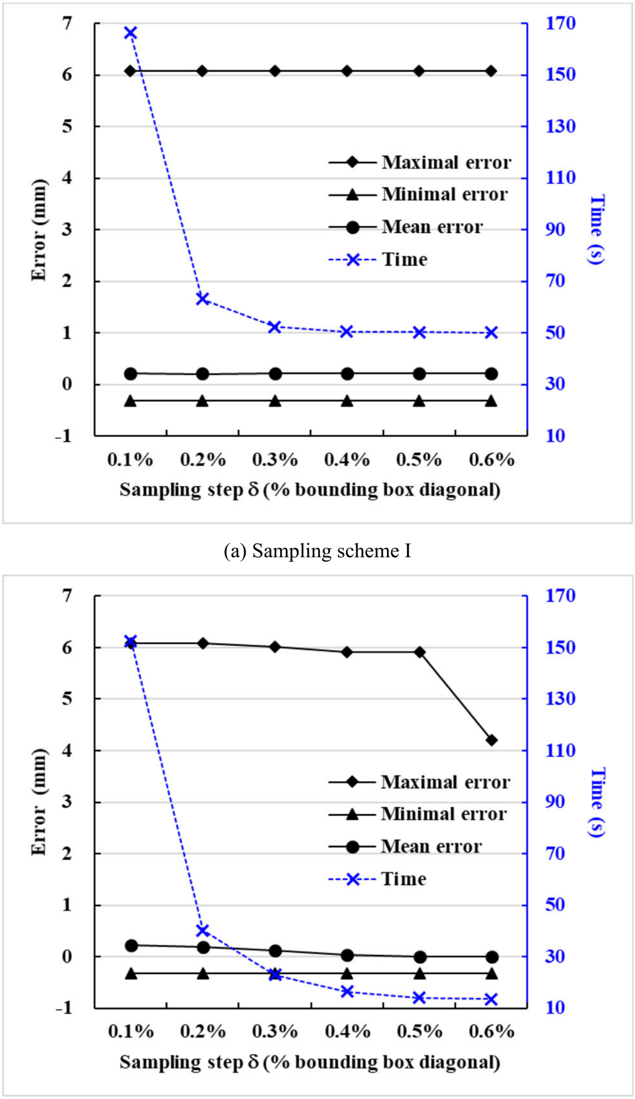

(a) Sampling scheme I

(b) Sampling scheme II

**Fig. 6** Comparison of the error and time with respect to different sampling schemes of the roughing model. **a** Sampling scheme I. **b** Sampling scheme II

## 4 Results and discussion

The proposed algorithm has been implemented in Unity 3D coded with C# as a verification module for the NC machining simulation system. The verification module runs on a personal computer with an Intel(R) Core(TM) i7-10710U CPU 1.10 GHz with 16.00-GB memory. In our previous work, the NC simulation of the core block of an injection mold

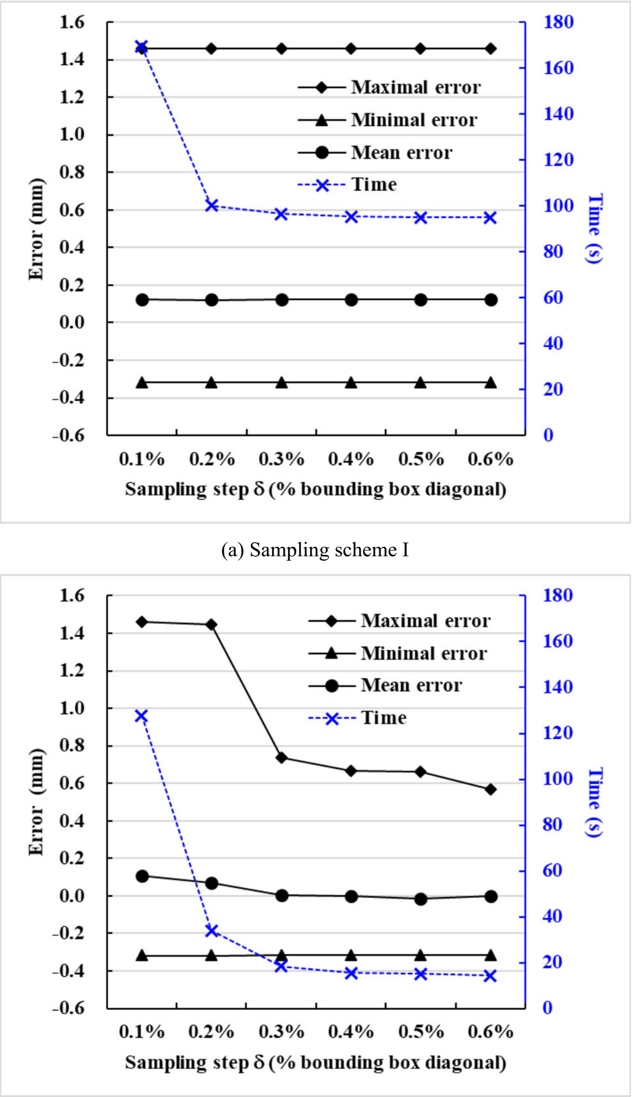

(a) Sampling scheme I

(b) Sampling scheme II

**Fig. 7** Comparison of the error and time with respect to different sampling schemes of the semifinishing model. **a** Sampling scheme I. **b** Sampling scheme II

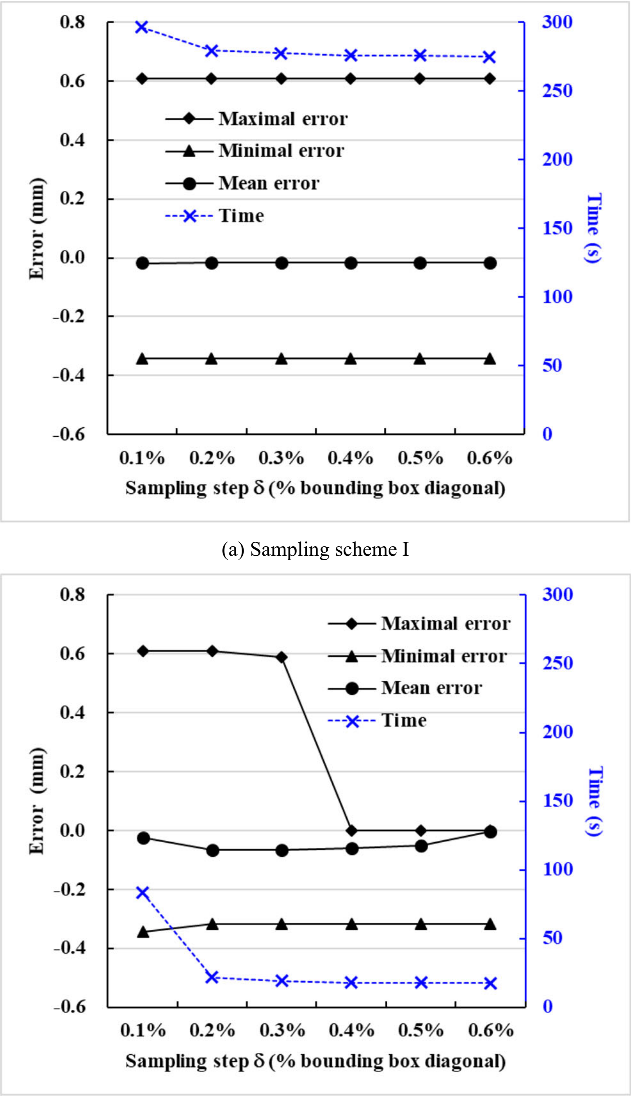

(a) Sampling scheme I

(b) Sampling scheme II

**Fig. 8** Comparison of the error and time with respect to the different sampling schemes of the finishing model. **a** Sampling scheme I. **b** Sampling scheme II

was carried out for performance evaluation, and the resulting roughing model, semifinishing model, and finishing model are used here to evaluate the NC machining verification algorithm. The approximate accuracy of the nominal STL model is 0.08 mm.

The influence of different sampling schemes on the accuracy of the NC machining verification algorithm is investigated and compared. Sampling scheme I represents all the triangles that are sampled, while sampling scheme II represents the tiny triangles that are not sampled because of the given sampling step. The maximal error, minimal error, and mean error as functions of sampling step $\delta$ in sampling scheme I applied to the roughing model, semifinishing model, and finishing model, as shown in Figs. 6a, 7a, and 8a, respectively, remain stable, while they change with sampling step $\delta$ in sampling scheme II, as shown in Figs. 6b, 7b, and 8b. It can be concluded that in scheme II, the algorithm accuracy is sensitive to sampling step $\delta$, whereas the scheme I is not. This means that in scheme II, a small sampling step $\delta$ should be selected to improve the algorithm accuracy, but the computation time will be increased.

Although the maximal error and minimal error are the same in both sampling schemes I and II when sampling step $\delta$ is 0.1%, the differences in the mean error are approximately 2.39%, 14.04%, and 29.03% in the roughing model, semifinishing model, and finishing model, respectively, as the numbers of unsampled triangles in sampling scheme II are 108,385 (50.45% of total), 323,307 (68.71% of total), and 1,044,904 (84.31% of total), respectively, as shown in Table 1. It should be pointed out that the number of

**Table 1** Comparison of the sampling schemes I and II ($\delta$ = 0.1%)

| Sampling scheme | Roughing model | | Semifinishing model | | Finishing model | |
|---|---|---|---|---|---|---|
| | I | II | I | II | I | II |
| Time (s) | 166.587 | 152.634 | 169.43 | 127.79 | 296.304 | 83.332 |
| Maximal error (mm) | 6.0819 | 6.0819 | 1.4596 | 1.4596 | 0.6090 | 0.6090 |
| Minimal error (mm) | − 0.3173 | − 0.3173 | − 0.3173 | − 0.3173 | − 0.3437 | − 0.3437 |
| Mean error (mm) | 0.2219 | 0.2166 | 0.1234 | 0.1061 | − 0.0178 | − 0.0230 |
| Samples | 1,485,408 | 1,421,798 | 1,564,015 | 1,371,283 | 1,817,672 | 1,118,635 |
| Triangles not sampled | 0 | 108,385 | 0 | 323,307 | 0 | 1,044,904 |
| Total triangles | 214,822 | 214,822 | 470,537 | 470,537 | 1,239,420 | 1,239,420 |

unsampled triangles will increase as sampling step $\delta$ increases in sampling scheme II, which results in an inaccurate maximal error, minimal error, and mean error. Therefore, it can be concluded that the maximal error, minimal error, and mean error computed by sampling scheme II are not as accurate as those of sampling scheme I under the same sampling step $\delta$.

The influence of different sampling step $\delta$ on the efficiency of the NC machining verification algorithm is also investigated. The time needed to perform the algorithm first decreases remarkably as sampling step $\delta$ increases and then remains almost stable when $\delta$ is either 0.5% or 0.6% in sampling schemes I or II, as shown in Figs. 6, 7, and 8. It seems that both the accuracy and efficiency of the NC machining verification algorithm are optimal when sampling scheme I is adopted and the sampling step $\delta$ is set to 0.6% of the bounding box diagonal.

The error visualization is given by coloring the machined workpiece model according to the signed distance associated with each sample; therefore, the distribution of the error on the model can be observed clearly. The error visualization of the roughing model, semifinishing model, and finishing model in sampling scheme I with sampling step $\delta$ set to 0.1% are shown in Figs. 9, 10, and 11, respectively. In the error visualization, zero error, positive error, and negative error are represented by green, red, and blue, respectively. In other words, the machined workpiece has as much material as the nominal part in the green area, more material in the red area, and less material in the blue area. Therefore, the undercut and overcut areas can be easily detected in the sampling scheme I by error visualization if the error value falls out of the allowable tolerance zone. However, the undercut and overcut areas cannot be accurately detected in sampling scheme II because a non-negligible proportion of the very small triangles that accumulate at the cusps and gouges are not sampled.

Based on the above analysis, sampling scheme I is superior to sampling scheme II for three reasons: (1) the algorithm accuracy of sampling scheme I is robust to the sampling step $\delta$ while that of sampling scheme II is sensitive; (2) the maximal error, minimal error, and mean error computed by sampling scheme II are not as accurate as those of sampling scheme I under the same sampling step; (3) the undercut and overcut areas can be accurately detected by error visualization in sampling scheme I, but they cannot be completely detected by error visualization in sampling scheme II. Therefore, the improvement we made based on MESH [18] to sample all the triangles, including the very small triangles, is necessary and reasonable.

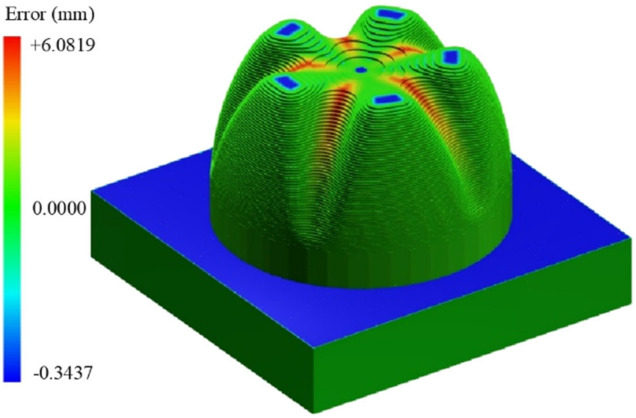

**Fig. 9** Error visualization of the roughing model (sampling scheme I, $\delta$ = 0.1%)

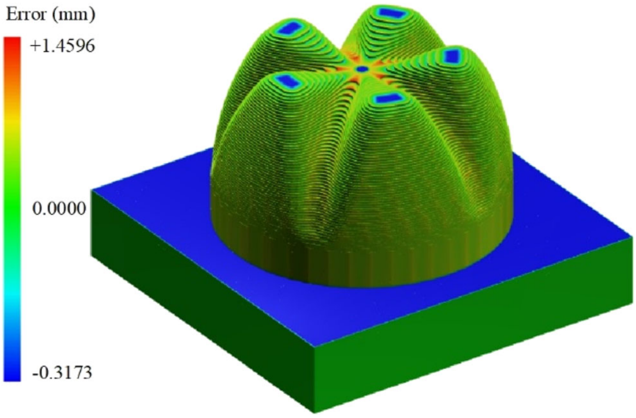

**Fig. 10** Error visualization of the semifinishing model (sampling scheme I, $\delta$ = 0.1%)

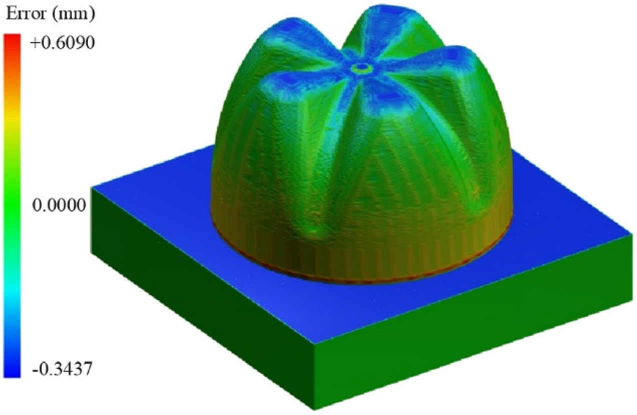

**Fig. 11** Error visualization of the finishing model (sampling scheme I, $\delta$ = 0.1%)

The worst-case computational complexity of the proposed algorithm depends on the sample number $n_s$ of the machined model $S_1$ and the triangle number $n_t$ of the nominal part $S_2$, and the resulting complexity is $O(n_s * n_t)$. In sampling scheme I, when the sampling step $\delta$ is 0.1%, the number of triangles tested to compute the minimal distance for each sample is 17,062 without applying the background grid; otherwise, only a few dozen of triangles are tested, as shown in Table 2. The ratios of the tested triangle numbers in these two cases are 302, 310, and 199 for the roughing model, semifinishing model, and finishing model, respectively, which means that the number of calculations of the signed distance for each sample can be reduced hundreds of times by applying the background grid. Therefore, the efficiency of the proposed algorithm is improved significantly.

## 5 Conclusion

The existing algorithms for evaluating the difference between two triangular meshes of similar shape are improved and applied for STL model-based NC machining verification, which consists of three steps: surface sampling, error evaluation, and background grid construction. In the improved algorithm, all the triangles including those that are too small to be sampled under the current sampling step $\delta$ are sampled to improve the verification accuracy; the signed distances are used to detect the undercut and overcut of the machined workpiece; and the background grid is applied to reduce the number of calculations of the signed distance for each sample. The experimental results demonstrate the accuracy and efficiency of the proposed NC machining verification algorithm based on STL models.

**Table 2** Efficiency improvement by applying the background grid (sampling scheme I, $\delta$ = 0.1%)

| | Triangles of $S_1$ | Triangles of $S_2$ | Samples | Tested triangles (per sample) | Ratio |
|---|---|---|---|---|---|
| Roughing | 214,822 | 17,062 | 1,485,408 | 56.5 | 302 |
| Semifinishing | 470,537 | | 1,564,015 | 55.1 | 310 |
| Finishing | 1,239,420 | | 1,817,672 | 85.8 | 199 |

**Funding information** The work reported in this paper is supported by the Science Fund for Creative Research Groups of the National Natural Science Foundation of China (No. 51821093), the National Key Research and Development Project of China (No. 2018YFC0808505), the Natural Science Foundation of the Jiangsu Higher Education Institutions of China (No. 19KJB460025), and the Jiangsu University-Industry Collaboration Project of China (No. BY2019043).

**Nomenclature** δ, sampling step; $n$, number of samples on each triangle side; $n'$, value of $n$ before rounded; $P(i,j)$, coordinate of the sample; $S_1$, machined workpiece model; $S_2$, nominal part; $T_1$, a triangle of $S_1$; $T_2$, a triangle of $S_2$; $P$, a sample; $d\ (p, T_2)$, signed distance between $p$ and $T_2$; $d\ (p, S_2)$, signed distance between $p$ and $S_2$; $d_{\max}\ (S_1, S_2)$, maximal error between $S_1$ and $S_2$; $d_{\min}\ (S_1, S_2)$, minimal error between $S_1$ and $S_2$; $d_{\text{mean}}\ (S_1, S_2)$, mean error between $S_1$ and $S_2$; $C$, the cell sample $p$ is located in; $\Delta d$, side length of the cubic cell; $m$, layer number of cells around $C$; $D_{\text{m}}\ (C)$, the set of cells that are at a distance $m * \Delta d$ from $C$ along with one of the coordinate axes

## References

1. Voelcker HB, Hunt WA (1981) The role of solid modeling in machining-process modeling and NC verification. SAE Technical Paper 810195.
2. Fleisig RV, Spence AD (2005) Techniques for accelerating B-rep based parallel machining simulation. Computer-Aided Design 37(12):1229–1240. https://doi.org/10.1016/j.cad.2004.11.008
3. Yang JZ, Abdel-Malek K (2006) Verification of NC machining processes using swept volumes. Int J Adv Manuf Technol 28(1-2):82–91. https://doi.org/10.1007/s00170-004-2352-8
4. Zhao G, Cao X, Xiao WL, Liu Q, Jun MBG (2020) STEP-NC feature-oriented high-efficient CNC machining simulation. Int J Adv Manuf Technol 106(5-6):2363–2375. https://doi.org/10.1007/s00170-019-04770-3
5. Lee SH, Lee KS (2002) Local mesh decimation for view-independent three-axis NC milling simulation. Int J Adv Manuf Technol 19(8):579–586. https://doi.org/10.1007/s001700200063
6. Aras E, Feng HY (2011) Vector model-based workpiece update in multi-axis milling by moving surface of revolution. Int J Adv Manuf Technol 52(9-12):913–927. https://doi.org/10.1007/s00170-010-2799-8
7. Joy J, Feng HY (2017) Efficient milling part geometry computation via three-step update of frame-sliced voxel representation workpiece model. Int J Adv Manuf Technol 92(5-8):2365–2378. https://doi.org/10.1007/s00170-017-0168-6
8. Kim YH, Ko SL (2006) Improvement of cutting simulation using the octree method. Int J Adv Manuf Technol 28(11-12):1152–1160. https://doi.org/10.1007/s00170-004-2462-3
9. Wang WP, Wang KK (1986) Geometric modeling for swept volume of moving solids. IEEE Comput Graph Appl 6(12):8–17. https://doi.org/10.1109/MCG.1986.276586

10. Sun YJ, Yan CY, Wu SW, Gong H, Lee CH (2018) Geometric simulation of 5-axis hybrid additive-subtractive manufacturing based on Tri-dexel model. Int J Adv Manuf Technol 99(9-12): 2597–2610. https://doi.org/10.1007/s00170-018-2577-6
11. Karunakaran KP, Shringi R (2007) Octree-to-BRep conversion for volumetric NC simulation. Int J Adv Manuf Technol 32(1-2):116–131. https://doi.org/10.1007/s00170-005-0310-8
12. Karunakaran KP, Shringi R, Ramamurthi D, Hariharan C (2010) Octree-based NC simulation system for optimization of feed rate in milling using instantaneous force model. Int J Adv Manuf Technol 46(5-8):465–490. https://doi.org/10.1007/s00170-009-2107-7
13. Yau HT, Tsou LS (2009) Efficient NC simulation for multi-axis solid machining with a universal APT cutter. J Comput Inf Sci Eng 9(2):375–389. https://doi.org/10.1115/1.3130231
14. Lee SW, Nestler A (2012) Virtual workpiece: workpiece representation for material removal process. Int J Adv Manuf Technol 58(5-8):443–463. https://doi.org/10.1007/s00170-011-3431-2
15. Miao Y, Song XW, Jin T, Shan Y (2016) Improving the efficiency of solid-based NC simulation by using spatial decomposition methods. Int J Adv Manuf Technol 87(1-4):421–435. https://doi.org/10.1007/s00170-016-8450-6
16. Tang M, Lee M, Kim YJ (2009) Interactive Hausdorff Distance computation for general polygonal models. ACM Trans Graph 28(3):9–9. https://doi.org/10.1145/1531326.1531380
17. Cignoni P, Rocchini C, Scopigno R (1998) Metro: measuring error on simplified surfaces. Comput Graph Forum 17(2):167–174. https://doi.org/10.1111/1467-8659.00236
18. Aspert N, Santa-Cruz D, Ebrahimi T (2002) MESH: measuring errors between surfaces using the Hausdorff distance. Ieee International Conference on Multimedia and Expo, Vol I and Ii, Proceedings:705-708. doi:https://doi.org/10.1109/icme.2002.1035879
19. Bartoň M, Hanniel I, Elber G, Kim MS (2010) Precise Hausdorff distance computation between polygonal meshes. Comput Aided Geom Des 27(8):580–591. https://doi.org/10.1016/j.cagd.2010.04.004
20. Kang Y, Kyung MH, Yoon SH, Kim MS (2018) Fast and robust Hausdorff distance computation from triangle mesh to quad mesh in near-zero cases. Comput Aided Geom Des 62:91–103. https://doi.org/10.1016/j.cagd.2018.03.017
21. Kang Y, Yoon SH, Kyung MH, Kim MS (2019) Fast and robust computation of the Hausdorff distance between triangle mesh and quad mesh for near-zero cases. Comput Graph-UK 81:61–72. https://doi.org/10.1016/j.cag.2019.03.014
22. Feito FR, Ogayar CJ, Segura RJ, Rivero ML (2013) Fast and accurate evaluation of regularized Boolean operations on triangulated solids. Computer-Aided Design 45(3):705–716. https://doi.org/10.1016/j.cad.2012.11.004
23. Gottschalk S, Lin MC, Manocha D (1996) OBBTree: a hierarchical structure for rapid interference detection. Paper presented at the Proceedings of the 23rd annual conference on Computer graphics and interactive techniques, New Orleans, August 4-9. doi:https://doi.org/10.1145/237170.237244